





# Spectral Analysis of Ceres' Main Linear Features

Andrea Longobardo <sup>1,\*</sup>, Filippo Giacomo Carrozzo <sup>1</sup>, Anna Galiano <sup>1</sup>, Jennifer E. C. Scully <sup>2</sup>, Rutu Parekh <sup>3</sup>, Ernesto Palomba <sup>1,4</sup>, Maria Cristina De Sanctis <sup>1</sup>, Eleonora Ammannito <sup>5</sup>, Andrea Raponi <sup>1</sup>, Federico Tosi <sup>1</sup>, Mauro Ciarniello <sup>1</sup>, Francesca Zambon <sup>1</sup>, Edoardo Rognini <sup>4,6</sup>, Maria Teresa Capria <sup>1,†</sup>, Carol A. Raymond <sup>2</sup> and Christopher T. Russell <sup>7</sup>

<sup>1</sup> Istituto di Astrofisica e Planetologia Spaziali (IAPS), Istituto Nazionale di Astrofisica (INAF), Via Fosso del Cavaliere 100, 00133 Rome, Italy

<sup>2</sup> Jet Propulsion Laboratory, California Institute of Technology, Pasadena, CA 91125, USA

<sup>3</sup> Deutsches Zentrum für Luft- und Raumfahrt (DLR), Institute for Planetary Research, D-12489 Berlin, Germany

<sup>4</sup> Space Science Data Center (SSDC), Agenzia Spaziale Italiana (ASI), 00133 Rome, Italy

<sup>5</sup> Unità di Ricerca Scientifica (URS), Agenzia Spaziale Italiana (ASI), 00133 Rome, Italy

<sup>6</sup> Osservatorio Astronomico di Roma (OAR), Istituto Nazionale di Astrofisica (INAF), 00078 Monteporzio Catone, Italy

<sup>7</sup> Department of Earth, Planetary, and Space Science, University of California, Los Angeles, CA 90025, USA

\* Correspondence: andrea.longobardo@inaf.it

† Deceased.

**Abstract:** Linear features are very common on asteroid surfaces. They are generally formed after impact and provide information about asteroid evolution. This work focuses on a mineralogical and spectral analysis of the main linear features on the 1/Ceres surface, having both tectonic (Samhain Catena's pit chains) and geomorphic origins, i.e., generated by ejecta material (Occator ejecta, Dantu's secondary radial chains, secondary radial chains generated from the Urvara impact). The analysis is based on spectral parameters defined by the Dawn's VIR imaging spectrometer data, as albedo and depths of the bands centered at approximately 2.7, 3.1, 3.4 and 3.9  $\mu\text{m}$ . The geomorphic linear features show spectral variations with respect to the surroundings, i.e., ammoniated phyllosilicates band depth shallowing is caused by the presence of material originating in a different region or dehydration caused by impact. The Samhain Catena does not show any mineralogical variation, due to its tectonic origin. The spectral behavior of Ceres' linear features is similar to that observed on other asteroids (Vesta, Eros) and can be diagnostic in discerning the origin of linear features. Then, we searched spectral signatures of organics in the Samhain Catena region, since they are expected to form at depth due to internal processes: the absence of such signatures indicates that either they form at a larger depth or that their subsurface distribution is uneven.

**Keywords:** Ceres; linear features; Dawn; spectroscopy



**Citation:** Longobardo, A.; Carrozzo, F.G.; Galiano, A.; Scully, J.E.C.; Parekh, R.; Palomba, E.; De Sanctis, M.C.; Ammannito, E.; Raponi, A.; Tosi, F.; et al. Spectral Analysis of Ceres' Main Linear Features. *Minerals* **2022**, *12*, 1013. <https://doi.org/10.3390/min12081013>

Academic Editor: Kattathu Mathew

Received: 23 May 2022

Accepted: 10 August 2022

Published: 12 August 2022

**Publisher's Note:** MDPI stays neutral with regard to jurisdictional claims in published maps and institutional affiliations.



**Copyright:** © 2022 by the authors. Licensee MDPI, Basel, Switzerland. This article is an open access article distributed under the terms and conditions of the Creative Commons Attribution (CC BY) license (<https://creativecommons.org/licenses/by/4.0/>).

## 1. Introduction

Our knowledge of the dwarf planet 1/Ceres has been greatly improved by the outcomes of NASA's Dawn mission [1], which acquired images, spectra and elemental maps of Ceres owing to its payload, utilizing a framing camera (FC) [2], visible and infrared mapping spectrometer (VIR) [3] and gamma ray and neutron detector (GRaND) [4].

Ceres is globally dark with an average I/F at a 30° phase of 0.03 both in the visible and in the near-infrared (NIR) spectral intervals [5], but it also presents some brighter spots [6]. Ceres' brightest areas are the Cerealia and Vinalia faculae located inside the Occator crater, with 0.55  $\mu\text{m}$  reflectance reaching values of up to 0.26 [7].

The Ceres spectra show absorption bands at 2.7, 3.1, 3.4 and 3.9  $\mu\text{m}$ , suggesting an average composition of magnesium-rich and ammoniated phyllosilicates (with the 2.7 and 3.1  $\mu\text{m}$  bands ascribed to OH and to ammonium, respectively), magnesium carbonates

(responsible for the bands at 3.4 and 3.9  $\mu\text{m}$ ) and a dark component [8]. The relative abundance of these components varies slightly across Ceres' surface, with the amount of carbonates increasing in brighter areas [9,10].

Nevertheless, there are some Ceres regions with a peculiar composition. The two Occator faculae (20° N 240° E) contain different types of phyllosilicates (aluminum instead of magnesium) and carbonates (sodium instead of magnesium), as revealed from the deepening and longward shift of the 2.7, 3.4 and 3.9  $\mu\text{m}$  bands [7,10]. The Juling (35° S 168° E) spectra showed water–ice absorption bands at 1.25, 1.5 and 2.0  $\mu\text{m}$ , and their depth changed with heliocentric distance, indicating a seasonal water cycle [11]. Spectra in a localized region, including rim and ejecta, of the Ernutet (52° N 45° E) crater show a 3.4  $\mu\text{m}$  deepening ascribed to the occurrence of aliphatic organics [12]. These could be the result of internal processes, although an exogenous origin has also been considered [13].

This work focuses on the spectral and mineralogical analysis of Ceres' linear features. These are very common features on small bodies [14] and are generally related to impact, thus providing information on the evolution of small bodies. Ref. [15] identified four main types of linear features on small bodies: troughs (i.e., depressions bounded by conjugate faults), ridges (i.e., chains of elevated regions forming a crest), modifications of crater shapes (rarely observed) and grooves. In turn, the latter can be divided depending on their origin: tectonic grooves include subtle topographic changes and fractures, while geomorphic grooves consist of ejecta material bouncing on the surface (e.g., secondary crater chains). A relation between the origin of linear features and spectral properties has been found in the literature. Except in a few cases of albedo markings, the tectonic linear features of Eros and Lutetia do not show distinctive spectral characteristics [16,17]. Vesta includes four types of linear features: graben, tectonic grooves, geomorphic grooves and ridges [18]. While graben and tectonic grooves are not associated with spectral variation, the albedo and pyroxene band depth changes observed in correspondence to geomorphic grooves indicate a different composition [17]. Vesta's ridges are instead characterized by a bluer color, which is probably associated with a fresher material [17].

On Ceres, two main types of linear features have been identified [19]: tectonic grooves, such as fractures and pit chains, and geomorphic grooves as secondary crater chains that are characterized by more defined rims, more regular shapes and a generally lower depth [19].

Here, we perform a spectral and mineralogical analysis of Ceres' longest linear features: four of them are geomorphic (features in the Dantu and Occator areas, Junina Catena, and Urvara ejecta), while one has tectonic origin (Samhain Catena). This analysis is based on the VIR data acquired at a spatial resolution down to 350–400 m/pixel; a study of smaller features based on high spatial resolution data will be the focus of a subsequent paper. Then, we will look for possible organic signatures in the feature sampling of Ceres' subsurface, since they are thought to be formed from internal processes.

## 2. Data

The VIR is the imaging spectrometer that was onboard the Dawn spacecraft [3]. It includes an optical head working in the visible (0.2–1  $\mu\text{m}$ , spectral sampling of 1.8 nm) and infrared (1–5  $\mu\text{m}$ , spectral sampling of 9.5 nm) intervals.

The spatial resolution changed as a function of the spacecraft's altitude on Ceres' surface. It was 3400 m/pixel during the Rotational Characterization (April–May 2015), 1100 m/pixel during the Survey (June 2015), approximately 400 m/pixel during the High Altitude Mapping Orbit (HAMO, August–October 2015) and approximately 100 m/pixel during the Low Altitude Mapping Orbit, which lasted until the end of the mission.

In this work, we considered spectra acquired during the HAMO phase, representing the best compromise between spatial coverage and spatial resolution.

The data reduction operations performed on the VIR spectra were the following: (i) calibration in radiance factor I/F (in the following, we refer to I/F also by using the term "reflectance") according to the procedure described by [20]; (ii) the removal of spectral artifacts, owing to an artifact matrix development [21]; (iii) the removal of thermal emission

contributions by applying the procedure described by [22]; and (iv) photometric correction to incidence, emission and phase angles of  $30^\circ$ ,  $0^\circ$ ,  $30^\circ$ , respectively, by means of the Hapke modeling [23], whose results have also been validated by comparison with those obtained from other photometric models [5].

### 3. Selection of Linear Features

The analysis was performed on the five most prominent linear features of Ceres. Four of them are of geomorphic origin (ejecta material bouncing on the surface), while the last has tectonic origin:

- *Dantu crater chains*. This group of secondary crater chains surrounds the Dantu crater, centered at  $24^\circ$  N  $138^\circ$  E. Chains extend radially from Dantu, especially west- and southwest-ward and, therefore, are thought to be generated from the impact producing the crater [24];
- *Occator ejecta*. This is the group of linear features generated from the Occator crater (centered at  $19^\circ$  N  $239^\circ$  E), which extends mainly south-ward from the crater [25,26];
- *Junina Catenae*. The Junina Catenae is a group of 11 secondary radial chains extending from  $12^\circ$  to  $46^\circ$  N and from  $95^\circ$  E to  $265^\circ$  E, oriented in directions WNW–ESE and crosscut by several impact craters (formed after the crater chains), including Dantu and Occator [19]. According to ejecta distribution models [27], the Junina Catenae formed from the material ejected with high velocity from the impact that formed the Urvara crater, located in the Southern Hemisphere, and is distributed in a nonradial pattern due to Ceres' rotation and low gravity;
- *Urvara secondary crater chains*. This is the set of crater chains formed by the material ejected from the Urvara crater, surrounding the crater itself, mainly in a north-ward direction. Differently than the Junina Catenae, these chains were formed from material ejected at low velocity, i.e., about 200 m/s [27];
- *Samhain Catenae*. Samhain Catenae are six pit chains extending between  $10^\circ$  S– $10^\circ$  N latitudes and  $210$ – $280^\circ$  E longitudes and are NW–SE-oriented [19]. Like the Junina Catenae, the Samhain Catenae are not radial with respect to impact craters. Nevertheless, their origin is not ascribed to high-velocity material ejected from an impact far from the current chains' location, but to surficial material draining into subsurface voids [19,25]. The surface stresses which generated these voids were likely due to a region of upwelling salt diapirs [25], but other hypotheses concern a basin-forming impact [28] and the freezing of a global subsurface ocean (thought to have occurred within hundreds of Myr after Ceres' formation, [29]).

The location of these linear features on Ceres is shown in Figure 1.

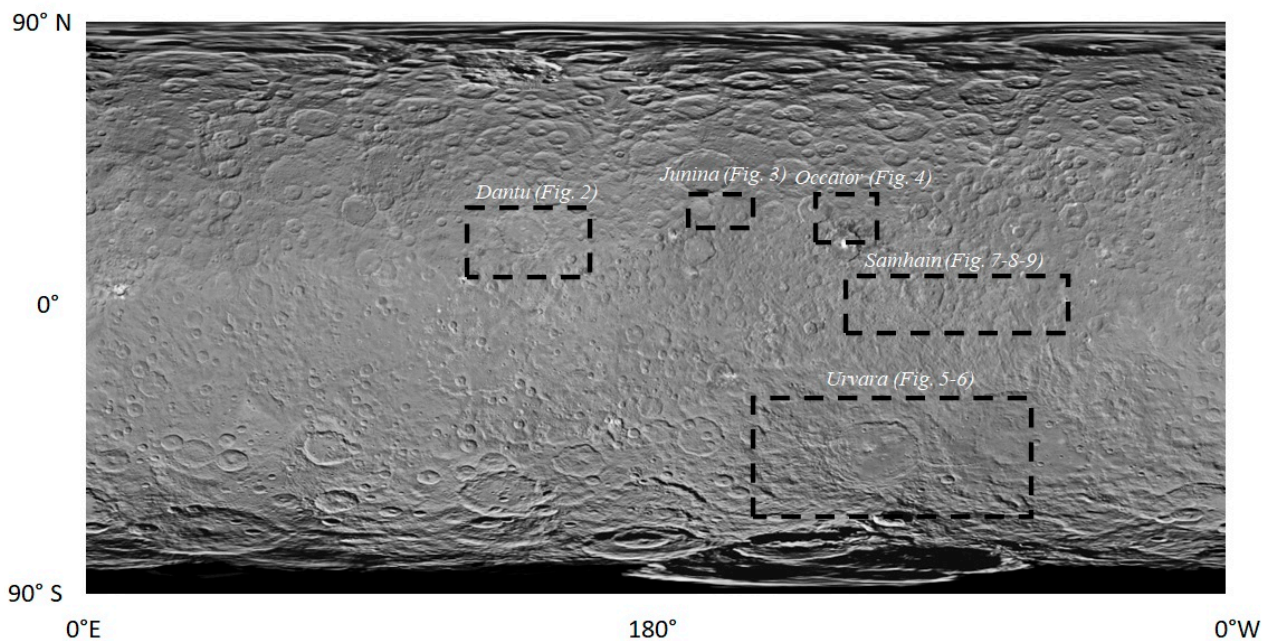


**Figure 1.** Location of linear features studied in this work over-imposed on the Ceres FC cylindrical map (USGS Astrogeology Science Center). Note that each square includes the areas imaged in the following figures, but each feature extends to wider areas. For the full features extension refer to [19].

#### 4. Spectral Maps

We studied the spatial distribution of the spectral parameters that are commonly used for the mineralogical analysis of Ceres' regions (e.g., [22,26,30–33]), which can have a significant spatial variability. These parameters were defined as in [5,34] and calculated on photometrically corrected spectra:

- NIR albedo is calculated at 1.2  $\mu\text{m}$  as the average between the four VIR closest bands to this wavelength in order to maximize the signal-to-noise ratio;
- All the band depths are calculated as  $1 - R_c/R_{\text{con}}$ , where  $R_c$  and  $R_{\text{con}}$  are the reflectance and the continuum at the band center wavelength (i.e., the local minimum after the continuum removal) [35]. The continuum is defined as the straight line connecting the two band shoulders. The band shoulders are calculated as follows:
  - For the 2.7  $\mu\text{m}$  band (ascribed to phyllosilicates), the left shoulder is the local maximum between 2.63 and 2.70  $\mu\text{m}$ , and the right shoulder is the reflectance maximum of the second-order polynomials fitting the spectra between 2.8 and 3.0  $\mu\text{m}$ ;
  - For the 3.1  $\mu\text{m}$  band (ascribed to ammoniated materials), the shoulders are the local maxima of the second-order polynomials fitting the spectra between 2.8 and 3.0  $\mu\text{m}$  and between 3.16 and 3.27  $\mu\text{m}$ , respectively;
  - For the 3.4  $\mu\text{m}$  band (Mg-carbonates, with the contribution of ammoniated materials), we considered the local maxima between 3.05–3.36  $\mu\text{m}$  and 3.55–3.68  $\mu\text{m}$ , respectively;
  - For the 3.9  $\mu\text{m}$  band (Mg-carbonates), we considered the local maxima between 3.55–3.68  $\mu\text{m}$  and 4.05–4.19  $\mu\text{m}$ .
- The spectral slope is defined as  $(R_{1.9} - R_{1.2})/R_{1.9}(1.9 - 1.2)$ , where  $R_\lambda$  is the reflectance at the wavelength  $\lambda$ .

Maps of these spectral parameters were produced for all of Ceres' regions considered in this work.

## 5. Results and Discussion

### 5.1. Dantu

The region containing Dantu's secondary crater chains shows shallow 2.7 and 3.1  $\mu\text{m}$  bands, with the lowest band depth values corresponding with the linear features (Figure 2). This agrees with the geomorphic origin of these linear features, which are expected to have a composition slightly different than their surroundings. In this case, the shallower band depths could indicate that the chains' material was dehydrated from the impact that generated the Dantu crater, and was then ejected in west and southwest directions. Nevertheless, a larger particle size could explain the observed spectral behavior in this region (e.g., [32]). Because Dantu is a quite recent crater (72–150 Ma, according to the Lunar-Derived Model, [24,36]), its secondary crater chains could show a different granulometry.

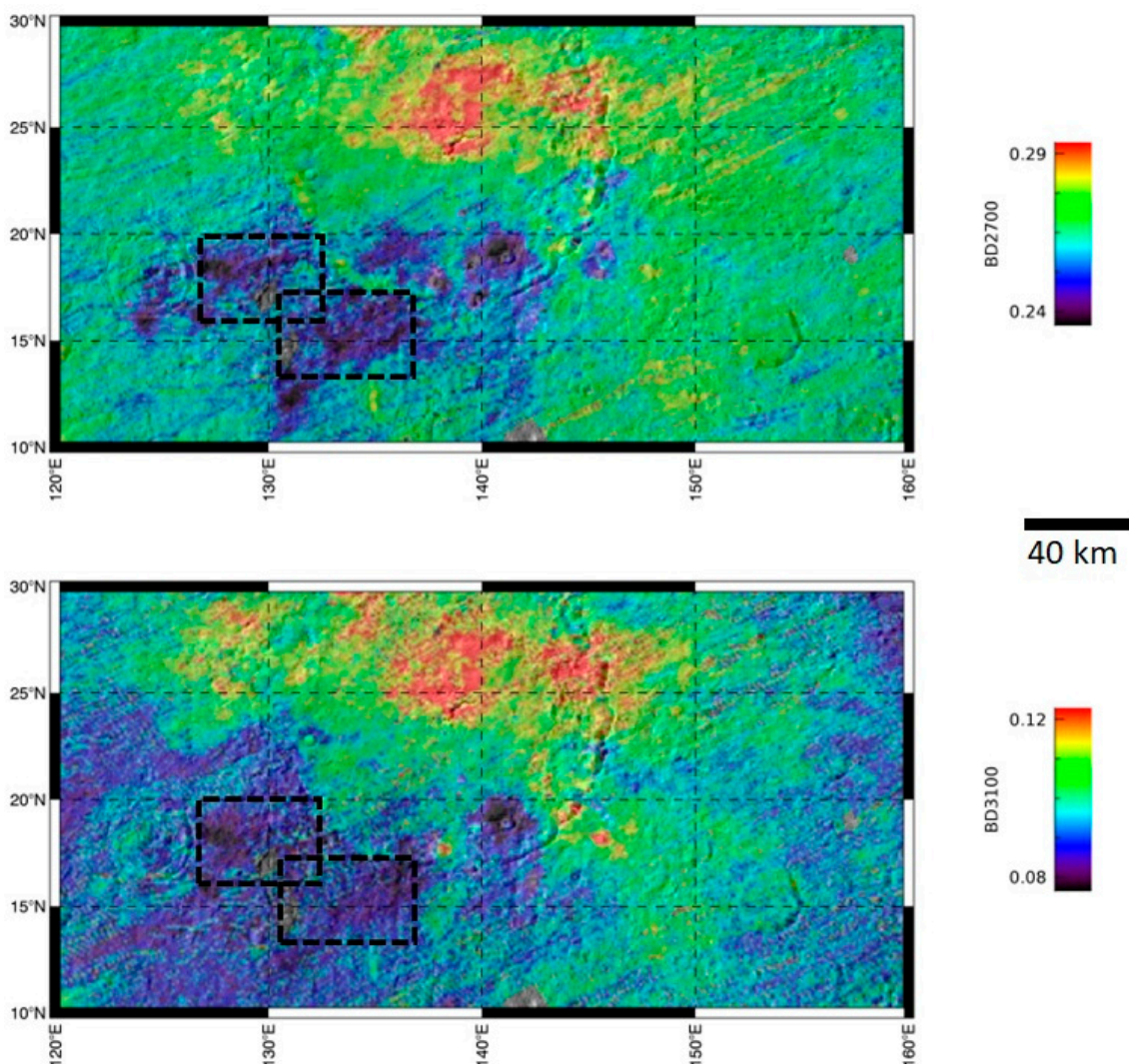


**Figure 2.** Distribution of the 2.7 and 3.1  $\mu\text{m}$  band depths in the Dantu region (cylindrical projection). The dotted squares enclose the linear features region. Scale bar refers to the latitude at the map center.

### 5.2. Junina Catena

#### 5.2.1. Far Ejecta

Most of the Junina Catena linear features are nonradial chains of impact craters, extending in to region between the Dantu and Occator craters. The nonradial pattern is due to the long travel time of ejecta generated by the Urvara impact (i.e., 6–8 h), comparable

with Ceres' rotation period (9 h) [27]. These features were preliminary characterized by [19], who found that the 2.7 and 3.1  $\mu\text{m}$  bands were shallower than the surroundings, suggesting a different material origin. We confirm this result here (Figure 3).

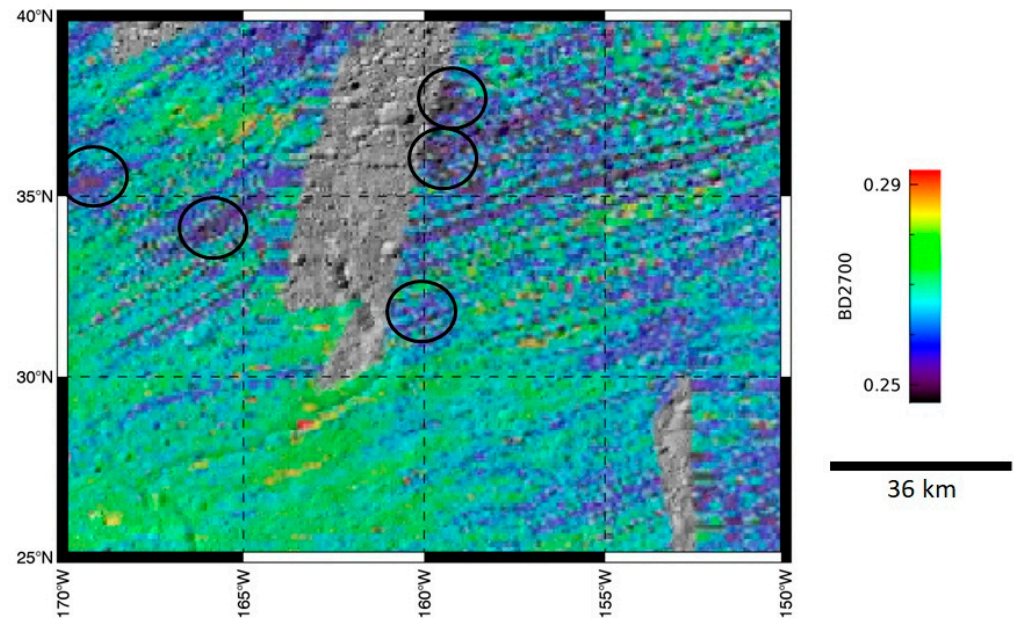


**Figure 3.** Spatial distribution of the 2.7  $\mu\text{m}$  band depth in the Junina Catenae region (cylindrical projection). Circles highlight linear features associated with shallowest bands. Scale bar refers to the latitude at the map center.

This agrees with the Junina Catenae formation from the material expelled (and then fallen back) from the Urvara region, which is one of Ceres' regions with the shallowest band depths [31].

#### 5.2.2. Occator Region Ejecta

The Junina Catenae also include nonradial furrows located to the north of the Occator crater. These features are also clearly recognizable from spectral maps, due not only to shallower band depths, but also to larger albedo (Figure 4). Since the Urvara crater albedo is larger than that observed in this region [31], this result further evidences that the Junina Catenae originated from the Urvara impact and that linear features of geomorphic origin can be observed from spectral maps. Moreover, the observed spectral parameter distribution is not consistent with a different grain size in the Junina Catenae region, because a larger grain size would produce the shallowing of both bands and an albedo decrease (e.g., [31]), which is different from our observations.

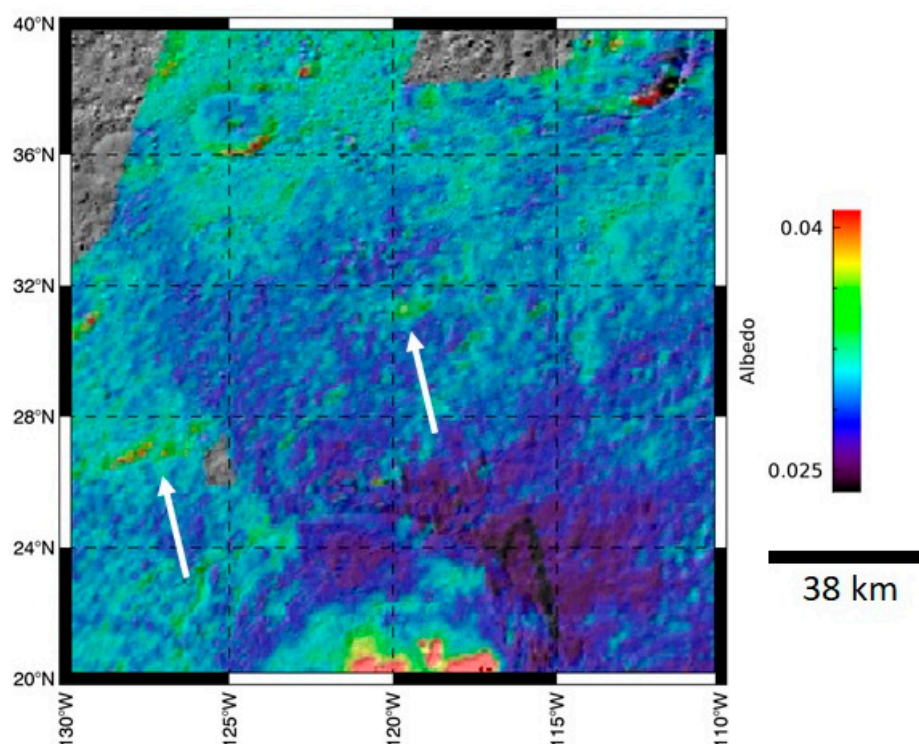


**Figure 4.** NIR albedo cylindrical map of the region north of the Occator crater. Arrows indicate an increase in albedo corresponding to the Junina Catenae linear feature locations. Scale bar refers to the latitude at the map center.

### 5.3. Occator Ejecta

The Occator southern and western ejecta include radial furrows. Ref. [26] concluded that these ejecta originated from the impact that generated the Occator crater, which is different from the eastern ejecta that are associated with the unnamed crater north of Occator.

The Occator ejecta show very shallow 2.7 and 3.1  $\mu\text{m}$  band depths, while the albedo is quite similar to the surroundings (for spectral maps, refer to [26]). Because the two bands are ascribed to OH and ammonium, we concluded that Occator's linear features are composed of materials that were ammonium-depleted and dehydrated from the impact, and then ejected from the crater.

### 5.4. Urvara Ejecta

The radial chains of impact craters and the radial furrows surrounding the Urvara crater do not have the same spectral behavior, because only a few of them are associated to 2.7  $\mu\text{m}$  and 3.1  $\mu\text{m}$  band depth variations, while others do not clearly emerge from band depth maps (e.g., Figure 5).

The lack of clear and common Urvara linear feature spectral behavior can be ascribed to the following reasons:

(a) The materials mixing in the Urvara region were stronger than those in other terrains due to the old age of this region, and in particular, the narrowest Urvara features may have lost their original spectral characteristics. Nonetheless, the Urvara ejecta in the northern and western Ceres regions (i.e., the Junina Catenae) are better evidenced in spectral maps, owing to Ceres' north–south and east–west spectral dichotomy [8];

(b) The VIR coverage of the Urvara region was not complete, and some observations were not considered in our work because of the large incidence/emission angles, meaning that spectra could not be photometrically corrected with a good accuracy.

Nonetheless, linear features not observable from the ammoniated phyllosilicates band depth maps are instead characterized by carbonate band depth markings (e.g., Figure 6). For example, the linear feature east of the crater contains some carbonate enrichments [9].

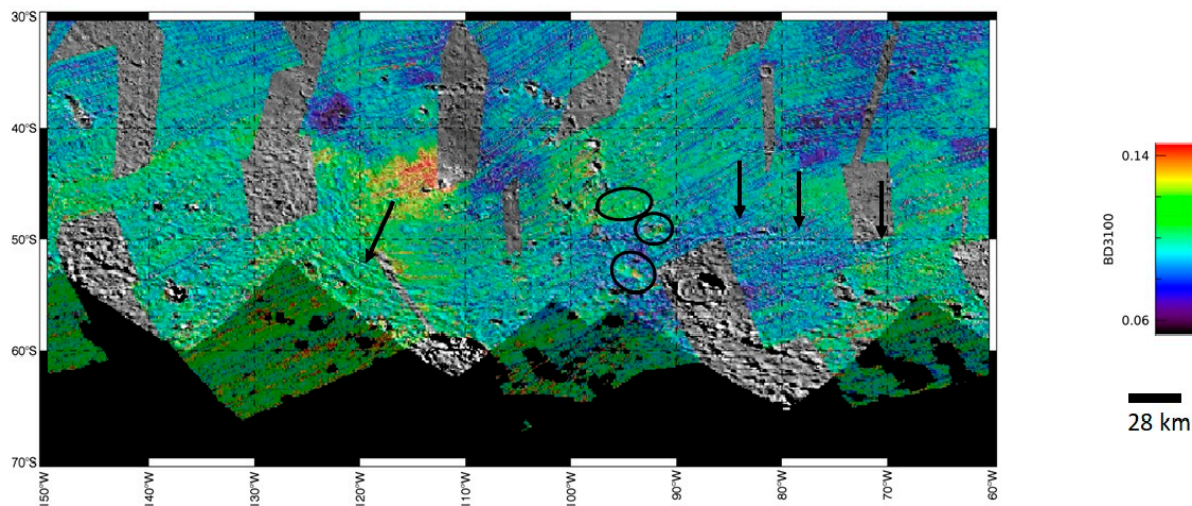


**Figure 5.** The 3.1  $\mu\text{m}$  band depth cylindrical map of the Urvara region (the 2.7 band depth map has a similar distribution). Arrows indicate linear feature locations: specifically, black circles indicate linear features showing a band depth different from the surroundings, while black arrows indicate features spectrally similar to the surroundings. Scale bar refers to the latitude at the map center.

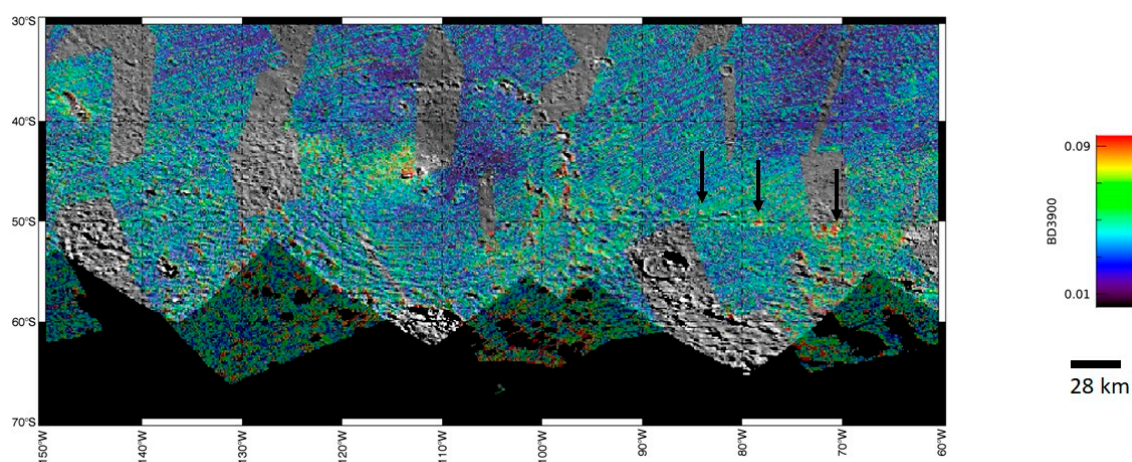


**Figure 6.** The 3.9  $\mu\text{m}$  band depth distribution of the Urvara region (3.4  $\mu\text{m}$  band depth distribution is similar) with arrows indicating carbonate enrichments in correspondence to linear features (cylindrical projection). Scale bar refers to the latitude at the map center.

### 5.5. Samhain Catena

The Samhain Catena is Ceres' main structural linear feature. Due to its origin, it is not expected to be associated with any spectral or compositional variation, as it is filled with surficial material draining into a subsurface. The 2.7 and 3.1  $\mu\text{m}$  band depth distributions confirm this expectation (Figure 7). Therefore, Ceres' tectonic features spectrally behave as those observed on other small bodies (e.g., Vesta, [17]).



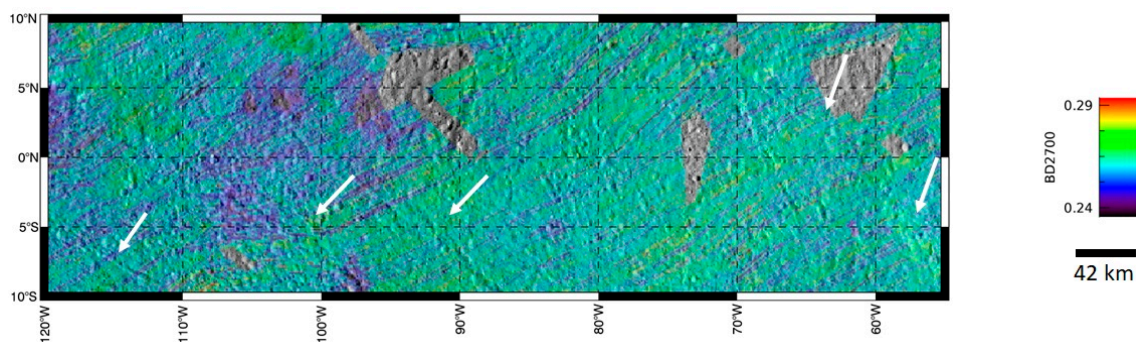


**Figure 7.** The 2.7  $\mu\text{m}$  band depth distribution of the Samhain Catenae region (cylindrical projection). The arrows indicate the linear features, which are not associated with band depth variations at all. Scale bar refers to the latitude at the map center.

Nonetheless, the eastern linear feature shows some albedo markings, being brighter than the surroundings (Figure 8). This behavior has already been observed on tectonic linear features of other small bodies, such as Vesta [17], Lutetia [37] and especially Eros [16]. This can be due to subsurface exposition, which is likely different than the surface. Another explanation is the occurrence of geological events which fill the pit chains with material moving downslope: this is the most claimed hypothesis for the albedo markings observed on the Eros linear features [16].

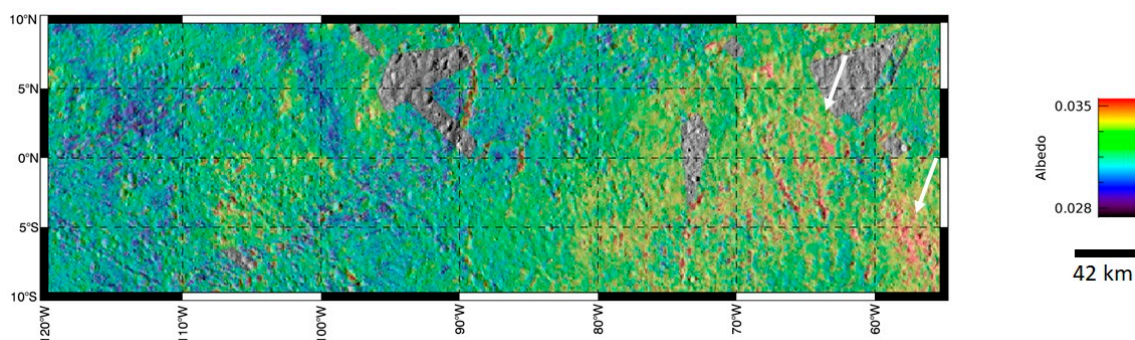


**Figure 8.** Albedo increase (highlighted by white arrows) observed in correspondence to the eastern feature of the Samhain Catenae (cylindrical projection).

### 5.6. Searching for Organic Signatures

Organic materials are supposed to have an endogenous origin on Ceres and are the result of internal processes, although the transfer process from interior to surface is not known [12,38].

Because of its structural origin, the Samhain Catenae are the only linear feature (among those studied here) that would allow the probing of Ceres' subsurface down to a depth of approximately 1 km (i.e., the feature depth). In order to clarify the organic presence in the subsurface, we looked for organic spectral signatures in this region by mapping the 3.4  $\mu\text{m}$  band depth.

The 3.4  $\mu\text{m}$  band depth distribution did not show any variation in correspondence to the Samhain Catenae linear features (Figure 9).

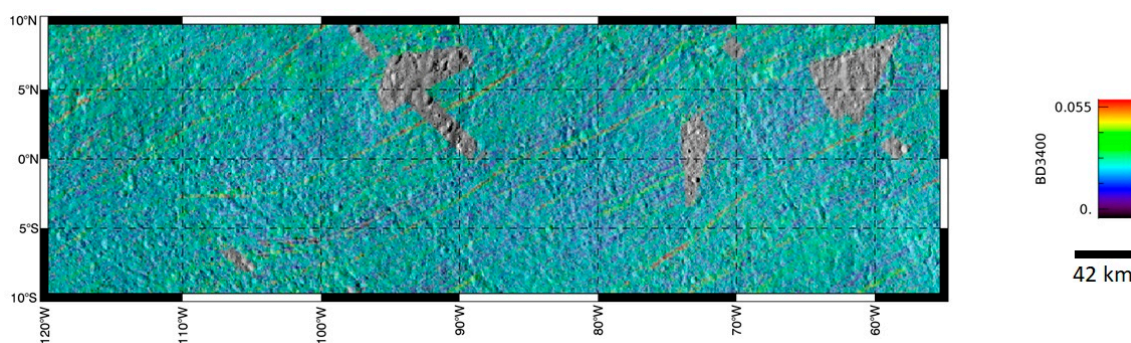


**Figure 9.** The 3.4  $\mu\text{m}$  band depth distribution of the Samhain Catenae region (cylindrical projection). No observable variations arise.

This suggests that organic material can form at locations deeper than 1 km or that their distribution on Ceres' subsurface is heterogeneous.

## 6. Conclusions

We produced spectral maps of Ceres' main linear features (Dantu, Occator, Urvara, Junina Catenae and Samhain Catenae) to observe variations in their spectral and mineralogical properties with respect to their surroundings.

As for other asteroids [16,17], we observed spectral variations, generally consisting of shallower 2.7 and 3.1  $\mu\text{m}$  absorption bands, in correspondence to geomorphic linear features. These are ascribed to material ejected from a region different than its actual location (Junina Catenae), to material dehydration (that results in shallower 2.7 and 3.1  $\mu\text{m}$  bands) caused by the impact generating the linear features (Occator, Dantu, Urvara), or to a different grain size, in the case of more recent features (Dantu). Spectral variations are less evident in older linear features (Urvara) and are likely due to subsequent mixing.

No mineralogical or spectral variations are observed in correspondence to the Samhain Catena, according to their tectonic origin, which did not imply a composition change. A few albedo markings are, however, observed due to subsurface exposition or downslope movements. The Samhain Catena would provide the opportunity to search organic spectral signatures at 1 km depth and to assess their formation depth; the absence of such signatures suggests that organics form at larger depths.

**Author Contributions:** Conceptualization, A.L.; Methodology, A.L., F.G.C., A.G., J.E.C.S., R.P., E.P., M.C.D.S., E.A., A.R., F.T., M.C., F.Z., E.R., M.T.C.; Validation, A.L.; Investigation, A.L., J.E.C.S.; Data curation, A.L., F.G.C., A.G., E.P., M.C.D.S., E.A., A.R., F.T., M.C., F.Z., E.R., M.T.C., C.T.R.; Writing—original draft, A.L.; writing—review and editing, A.L., A.G., R.P., C.T.R.; Visualization, C.T.R.; Project Administration, M.C.D.S., C.A.R., C.T.R.; Funding acquisition, M.C.D.S. All authors have read and agreed to the published version of the manuscript.

**Funding:** The VIR project is funded by the Italian Space Agency (ASI), ASI-INAF Contract I/004/12/0.

**Institutional Review Board Statement:** Not applicable.

**Informed Consent Statement:** Not applicable.

**Data Availability Statement:** Dawn data are archived in NASA's Planetary Data System; VIR spectral data may be obtained at: <https://sbn.psi.edu/pds/resource/dawn/> (accessed on 12 July 2022).

**Acknowledgments:** VIR was developed under the leadership of the Istituto di Astrofisica e Planetologia Spaziali (INAF-IAPS), Rome, Italy. The instrument was built by Selex-Galileo, Florence, Italy. Support of the Dawn Science, Instrument, Operations Teams, as well as of the Dawn at Vesta Participating Scientist program, is gratefully acknowledged. We also acknowledge the hard work carried out by Robert Gaskell in providing a detailed shape model that was used in this work to properly model the data.

**Conflicts of Interest:** The authors declare no conflict of interest.

## References

1. Russell, C.T.; Raymond, C.A. The Dawn Mission to Vesta and Ceres. *Space Sci. Rev.* **2011**, *163*, 3–23. [[CrossRef](#)]
2. Sierks, H.; Keller, H.U.; Jaumann, R.; Michalik, H.; Behnke, T.; Bubenhausen, F.; Büttner, I.; Carsenty, U.; Christensen, U.; Enge, R.; et al. The Dawn Framing Camera. *Space Sci. Rev.* **2011**, *163*, 263–327. [[CrossRef](#)]
3. De Sanctis, M.C.; Coradini, A.; Ammannito, E.; Filacchione, G.; Capria, M.T.; Fonte, S.; Magni, G.; Barbis, A.; Bini, A.; Dami, M.; et al. The VIR Spectrometer. *Space Sci. Rev.* **2011**, *163*, 329–369. [[CrossRef](#)]
4. Prettyman, T.H.; Feldman, W.C.; McSween, H.Y., Jr.; Dingler, R.D.; Enemark, D.C.; Patrick, D.E.; Storms, S.A.; Hendricks, J.S.; Morgenthaler, J.P.; Pitman, K.M.; et al. Dawn’s Gamma Ray and Neutron Detector. *Space Sci. Rev.* **2011**, *163*, 371–459. [[CrossRef](#)]
5. Longobardo, A.; Palomba, E.; Galiano, A.; De Sanctis, M.C.; Ciarniello, M.; Raponi, A.; Tosi, F.; Schröder, S.E.; Carrozzo, F.G.; Ammannito, E.; et al. Photometry of Ceres and Occator faculae as inferred from VIR/Dawn data. *Icarus* **2019**, *320*, 97–109. [[CrossRef](#)]
6. Stein, N.T.; Ehlman, B.L.; Palomba, E.; De Sanctis, M.C.; Nathues, A.; Hiesinger, H.; Ammannito, E.; Raymond, C.A.; Jaumann, R.; Longobardo, A.; et al. The formation and evolution of bright spots on Ceres. *Icarus* **2019**, *320*, 188–201. [[CrossRef](#)]
7. De Sanctis, M.C.; Raponi, A.; Ammannito, E.; Ciarniello, M.; Toplis, M.J.; McSween, H.Y., Jr.; Castillo-Rogez, J.C.; Ehlmann, B.L.; Carrozzo, F.G.; Marchi, S.; et al. Bright carbonate deposits as evidence of aqueous alteration on (1) Ceres. *Nature* **2016**, *536*, 54–57. [[CrossRef](#)]
8. Ammannito, E.; De Sanctis, M.C.; Ciarniello, M.; Frigeri, A.; Carrozzo, F.G.; Combe, J.-P.; Ehlmann, B.E.; Marchi, S.; McSween, H.Y.; Raponi, A.; et al. Distribution of phyllosilicates on the surface of Ceres. *Science* **2016**, *353*, aaf4279. [[CrossRef](#)]
9. Carrozzo, F.G.; De Sanctis, M.C.; Raponi, A.; Ammannito, E.; Castillo-Rogez, J.; Ehlmann, B.E.; Marchi, S.; Stein, N.; Ciarniello, M.; Tosi, F.; et al. Nature, formation and distribution of Carbonates on Ceres. *Sci. Adv.* **2018**, *4*, 447. [[CrossRef](#)]
10. Palomba, E.; Longobardo, A.; De Sanctis, M.C.; Stein, N.T.; Ehlmann, B.; Galiano, A.; Raponi, A.; Ciarniello, M.; Ammannito, E.; Cloutis, E.; et al. Compositional differences among Bright Spots on the Ceres surface. *Icarus* **2019**, *320*, 202–212. [[CrossRef](#)]
11. Raponi, A.; De Sanctis, M.C.; Frigeri, A.; Ammannito, E.; Ciarniello, M.; Formisano, M.; Combe, J.P.; Magni, G.; Tosi, F.; Carrozzo, F.G.; et al. Variations in the amount of water ice on Ceres’ surface suggest a seasonal water cycle. *Sci. Adv.* **2018**, *4*, eaao3757. [[CrossRef](#)] [[PubMed](#)]
12. De Sanctis, M.C.; Ammannito, E.; McSween, H.Y.; Raponi, A.; Marchi, S.; Capaccioni, F.; Capria, M.T.; Carrozzo, F.G.; Ciarniello, M.; Fonte, S.; et al. Localized aliphatic organic material on the surface of Ceres. *Science* **2017**, *355*, 719–722. [[CrossRef](#)] [[PubMed](#)]
13. Pieters, C.M.; Nathues, A.; Thangjam, G.; Hoffman, M.; Platz, T.; De Sanctis, M.C.; Ammannito, E.; Tosi, F.; Zambon, F.; Pasckert, J.H.; et al. Geologic constraints on the origin of red organic-rich material on Ceres. *Meteorit. Planet. Sci.* **2018**, *53*, 1983–1998. [[CrossRef](#)]
14. Hargitai, H.; Kereszturi, A. *Encyclopedia of Planetary Landforms*; Springer: Berlin/Heidelberg, Germany, 2015; ISBN 978-1-4614-3133-6.
15. Thomas, P.C.; Prockter, L.M. Tectonics of small bodies. In *Planetary Tectonics*; Watters, T.R., Schultz, R.A., Eds.; Cambridge University Press: Cambridge, UK, 2010.
16. Prockter, L.; Thomas, P.; Robinason, M.; Joseph, J.; Milne, A.; Bussey, B.; Veverka, J.; Cheng, A. Surface expressions of structural features on Eros. *Icarus* **2002**, *155*, 75–93. [[CrossRef](#)]
17. Longobardo, A.; Palomba, E.; De Sanctis, M.C.; Zinzi, A.; Scully, J.E.C.; Capaccioni, F.; Tosi, F.; Zambin, F.; Ammannito, E.; Combe, J.P.; et al. Mineralogical and spectral analysis of Vesta’s Gegania and Lucaria quadrangles and comparative analysis of their key features. *Icarus* **2015**, *259*, 72–90. [[CrossRef](#)]
18. Scully, J.E.C.; Yin, A.; Russell, C.T.; Buczkowski, D.L.; Williams, D.A.; Blewett, D.A.; Ruesch, O.; Hiesinger, H.; Le Corre, L.; Mercer, C.; et al. Geomorphology and structural geology of Saturnalia Fossae and adjacent structures in the northern hemisphere of Vesta. *Icarus* **2014**, *244*, 23–40. [[CrossRef](#)]
19. Scully, J.E.C.; Buczkowski, D.L.; Schememann, N.; Raymond, C.A.; Castillo-Rogez, J.C.; King, S.D.; Bland, M.T.; Ermakov, A.I.; O’Brien, D.P.; Marchi, S.; et al. Evidence for the Interior Evolution of Ceres from Geologic Analysis of Fractures. *Geophys. Res. Lett.* **2017**, *44*, 9564–9572. [[CrossRef](#)]
20. Filacchione, G.; Ammannito, E. Dawn VIR Calibration Document Version 2.4. 2014. Available online: [https://sbn.psi.edu/archive/dawn/vir/DWNVVIR\\_I1B/DOCUMENT/VIR\\_CALIBRATION/VIR\\_CALIBRATION\\_V2\\_4.PDF](https://sbn.psi.edu/archive/dawn/vir/DWNVVIR_I1B/DOCUMENT/VIR_CALIBRATION/VIR_CALIBRATION_V2_4.PDF) (accessed on 12 July 2022).
21. Carrozzo, F.G.; Raponi, A.; De Sanctis, M.C.; Ammannito, E.; Guardino, M.; D’Aversa, E.; Fonte, S.; Tosi, F. Artifacts reduction in VIR/Dawn data. *Rev. Sci. Instrum.* **2016**, *87*, 124501. [[CrossRef](#)]
22. Raponi, A.; Carrozzo, F.G.; Zambon, F.; De Sanctis, M.C.; Ciarniello, M.; Frigeri, A.; Ammannito, E.; Tosi, F.; Combe, J.-P.; Longobardo, A.; et al. Mineralogical mapping of Coniraya quadrangle of the dwarf planet Ceres. *Icarus* **2019**, *318*, 99–110. [[CrossRef](#)]
23. Ciarniello, M.; De Sanctis, M.C.; Ammannito, E.; Raponi, A.; Longobardo, A.; Palomba, E.; Carrozzo, F.G.; Tosi, F.; Li, J.-Y.; Schröder, S.E.; et al. Spectrophotometric properties of dwarf planet Ceres from VIR onboard Dawn mission. *Astron. Astrophys.* **2017**, *598*, A130. [[CrossRef](#)]
24. Stephan, K.; Jaumann, R.; Wagner, R.; De Sanctis, M.C.; Palomba, E.; Longobardo, A.; Williams, D.A.; Krohn, K.; Tosi, F.; McFadden, L.A.; et al. Dantu’s mineralogical properties—A view into the composition of Ceres’ crust. *Meteorit. Planet. Sci.* **2018**, *53*, 1866–1883. [[CrossRef](#)]

25. Buczkowski, D.L.; Schmidt, B.E.; Williams, D.A.; Mest, S.C.; Scully, J.E.C.; Ermakov, A.I.; Preusker, F.; Schenk, P.; Otto, K.A.; Hiesinger, H.; et al. The geomorphology of Ceres. *Science* **2016**, *353*, 1004. [[CrossRef](#)] [[PubMed](#)]
26. Longobardo, A.; Palomba, E.; Carrozzo, F.G.; Galiano, A.; De Sanctis, M.C.; Stephan, K.; Tosi, F.; Raponi, A.; Ciarniello, M.; Zambon, F.; et al. Mineralogy of the Occator quadrangle. *Icarus* **2019**, *318*, 205–211. [[CrossRef](#)]
27. Schmedemann, N.; Neesemann, A.; Schulzeck, F.; Krohn, K.; von der Gathen, I.; Otto, K.A.; Jaumann, R.; Michael, G.; Raymond, C.A.; Russell, C.T. The distribution of impact ejecta on Ceres. *Lunar Planet. Sci. Conf.* **2017**, *48*, 1233.
28. Marchi, S.; Ermakov, A.I.; Raymond, C.A.; Fu, R.R.; O'Brien, D.P.; Bland, M.T.; Ammannito, E.; De Sanctis, M.C.; Bowling, T.; Schenk, P.; et al. The missing large impact craters on Ceres. *Nat. Commun.* **2016**, *7*, 1–9. [[CrossRef](#)]
29. Castillo-Rogez, J.C.; Bowling, T.; Fu, R.R.; McSween, H.Y.; Raymond, C.A.; Rambaux, R.; Travis, B.; Marchi, S.; O'Brien, D.P.; Johnson, B.C.; et al. Loss of Ceres' icy shell from impacts: Assessment and implications. *Lunar Planet. Sci. Conf.* **2016**, *47*, 3012.
30. De Sanctis, M.C.; Frigeri, A.; Ammannito, E.; Carrozzo, F.G.; Ciarniello, F.; Zambon, F.; Tosi, F.; Raponi, A.; Longobardo, A.; Combe, J.P.; et al. Ac-H-11 Sintana and Ac-H-12 Toharu quadrangles: Assessing the large and small scale heterogeneities of Ceres' surface. *Icarus* **2019**, *318*, 230–240. [[CrossRef](#)]
31. Longobardo, A.; Galiano, A.; Ammannito, E.; Carrozzo, F.G.; De Sanctis, M.C.; Palomba, E.; Zambon, F.; Frigeri, A.; Ciarniello, M.; Raponi, A.; et al. Mineralogy of the Urvara-Yalode region on Ceres. *Icarus* **2019**, *318*, 241–250. [[CrossRef](#)]
32. Palomba, E.; Longobardo, A.; De Sanctis, M.C.; Carrozzo, F.G.; Galiano, A.; Zambon, F.; Raponi, A.; Ciarniello, M.; Stephan, K.; Williams, D.A.; et al. Mineralogical mapping of the Kerwan quadrangle on Ceres. *Icarus* **2019**, *318*, 188–194. [[CrossRef](#)]
33. Zambon, F.; Carrozzo, F.G.; Tosi, F.; Ciarniello, M.; Combe, J.-P.; Frigeri, A.; De Sanctis, M.C.; Thangjam, G.; Nathues, A.; Hoffmann, M.; et al. Mineralogical analysis of quadrangle Ac-H-10 Rongo on the dwarf planet Ceres. *Icarus* **2019**, *318*, 212–219. [[CrossRef](#)]
34. Galiano, A.; Palomba, E.; Longobardo, A.; Zinzi, A.; De Sanctis, M.C.; Raponi, A.; Carrozzo, F.G.; Ciarniello, M.; Dirri, F. Continuum definition for  $\sim 3.05$ ,  $\sim 3.4$  and  $\sim 4.0$   $\mu\text{m}$  absorption bands in Ceres spectra and evaluation of effects of smoothing procedure in the retrieved spectral parameters. *Adv. Space Res.* **2018**, *62*, 2342–2354. [[CrossRef](#)]
35. Clark, R.N.; Roush, T.L. Reflectance spectroscopy—Quantitative analysis techniques for remote sensing applications. *J. Geophys. Res.* **1984**, *89*, 6329–6340. [[CrossRef](#)]
36. Williams, D.A.; Kneissl, T.; Neesemann, A.; Mest, S.C.; Palomba, E.; Platz, T.; Nathues, A.; Longobardo, A.; Scully, J.E.C.; Ermakov, A.; et al. The geology of Kerwan quadrangle of dwarf planet Ceres: Investigating Ceres' oldest, largest impact basin. *Icarus* **2018**, *316*, 99–113. [[CrossRef](#)]
37. Thomas, N.; Barbieri, C.; Keller, H.U.; Lamy, P.; Rockman, H.; Rodrigo, R.; Sierks, H.; Wenzel, K.P.; Cremonese, G.; Jorda, L.; et al. The geomorphology of (21) Lutetia: Results from the OSIRIS imaging system onboard ESA's Rosetta spacecraft. *Planet. Space Sci.* **2012**, *66*, 96–124. [[CrossRef](#)]
38. Domagal-Goldman, S.D.; Wright, K.E.; Adamala, K.; de La Rubia, L.A.; Bond, J.; Datrnell, L.R.; Goldman, A.D.; Lynch, K.; Naud, M.-E.; Paulino-Lima, I.G.; et al. The Astrobiology Primer v2.0. *Astrobiology* **2016**, *16*, 561. [[CrossRef](#)] [[PubMed](#)]